Experimental Eye Research 264 (2026) 110824

Contents lists available at ScienceDirect

Experimental Eye Research

journal homepage: www.elsevier.com/locate/yexer

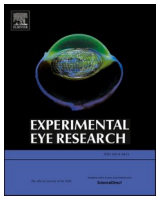

Research article

# Effect of increasing chain length on inhibition of evaporation by perfluoro compounds in an in vitro gravimetric assay

Megan E. Cavet [a], Jason L. Vittitow [b], Douglas Borchman [c,*]

[a] Bausch + Lomb, Rochester, NY, USA
[b] Bausch + Lomb, Bridgewater, NJ, USA
[c] Department of Ophthalmology and Visual Sciences, University of Louisville, Louisville, KY, USA

ARTICLE INFO

*Keywords:*
Dry eye
Evaporation
Perfluorohexyloctane
Semifluorinated alkane
Tear film

ABSTRACT

*Objective:* Semifluorinated alkanes (SFAs) are amphiphilic molecules with a fluorinated carbon segment (F) and a hydrocarbon segment (H). Perfluorohexyloctane ophthalmic solution (F6H8; MIEBO®) is an anti-evaporative agent for dry eye that forms a long-lasting layer on the surface of the tear film. This in vitro study evaluated the impact of SFA chain length on intermolecular interactions, evaporation rate ($R_{evap}$), and inhibition of $R_{evap}$ of saline to compare the anti-evaporative properties of various SFAs.

*Methods:* The SFAs F4H2, F4H5/CsA (cyclosporine ophthalmic solution 0.1 %; Vevye®), F6H7, F6H8, and F6H10 were evaluated. The $R_{evap}$ of 1 mL of each SFA and saline alone or saline with 11 or 100 μL of the SFA layered over top were evaluated gravimetrically at 35 °C. Total sample weight was recorded every 10 min over 100 min, and $R_{evap}$ was obtained from the slope of the best-fit line obtained by least squares linear regression analysis. The relative order (fluidity) of the SFAs was evaluated using Fourier transform infrared spectroscopy.

*Results:* The mean (SEM) inherent $R_{evap}$ (mg/min) was 102 (25), 6.0 (0.6), 0.58 (0.20), 0.15 (0.017), and 0.12 (0.09) for F4H2, F4H5/CsA, F6H7, F6H8, and F6H10, respectively (n = 3–9). The $R_{evap}$ of saline with a 100 μL F6H7, F6H8, and F6H10 layer was inhibited by 40 %, 80 %, and 66 %, respectively ($p < 0.001$ vs saline), and unchanged by F4H2 and F4H5/CsA. Only F6H8 had a significant inhibitory effect on $R_{evap}$ of saline when applying an 11 μL drop ($p < 0.0001$ vs saline; n = 10–25). The SFA-SFA intermolecular interactions were greater with longer H and F chain lengths.

*Conclusions:* SFA chain length and volatility correlated with inhibition of the $R_{evap}$ of saline with the longest chain length SFAs F6H8 and F6H10 having the maximal effect. These data support the suitability of F6H8 as a treatment for evaporative dry eye disease.

## 1. Introduction

Dry eye disease is a common chronic disease of the ocular surface that results in damage to the cornea and conjunctiva and is associated with symptoms such as burning/stinging, eye irritation, and blurred vision. A leading driver of the disease is desiccation stress due to an insufficient tear film lipid layer, with 50 % of dry eye disease cases due to excessive evaporation caused by Meibomian gland dysfunction and an additional approximately 40 % having an evaporative component (Lemp et al., 2012). Perfluorohexyloctane was approved by the US Food and Drug Administration in 2023 for the treatment of signs and symptoms of dry eye disease (Schmidl et al., 2020; Habbe et al., 2023; Groβ and Kaercher, 2021; Steven et al., 2015, 2017; Eberwein et al., 2020; Sheppard et al., 2023; Tauber et al., 2021, 2023; Bacharach et al., 2025). Perfluorohexyloctane belongs to the class of semifluorinated alkanes (SFAs) that are colorless nonaqueous liquids consisting of 2 mutually phobic covalently linked moieties, a lipophobic perfluorocarbon segment, and a lipophilic hydrocarbon segment (Fig. 1). It reduces tear evaporation (Vittitow et al., 2023) by forming a long-lasting (Millar et al., 2025) layer at the air-liquid interface of the dysfunctional tear film lipid layer, a key contributor to the etiology of evaporative dry eye disease (Borchman, 2021; Nguyen et al., 2024; Borchman et al., 2011; Georgiev et al., 2017; Nagar et al., 2023). As a single-component, nonaqueous eye drop, the product is preservative free and does not have a pH or cations to carefully balance, an advantage over aqueous eye drops where such factors may cause stinging and irritation. Besides

* Corresponding author. The University of Louisville, Department of Ophthalmology and Visual Sciences 301 E Muhammad Ali Blvd, Louisville, KY, 40202, USA.
*E-mail address:* douglas.borchman@louisville.edu (D. Borchman).

https://doi.org/10.1016/j.exer.2025.110824
Received 12 August 2025; Received in revised form 16 December 2025; Accepted 21 December 2025
Available online 22 December 2025

the use of perfluorohexyloctane as a treatment for dry eye disease, SFAs are used as endotamponades in vitreoretinal surgery and as drug delivery vehicles and have been evaluated for other clinical applications such as oxygen carriers in blood substitutes (Tsagogiorgas and Otto, 2023).

The SFAs are amphiphilic (the 2 moieties have unlike affinities), amphisteric (the 2 moieties have different conformations and space requirements), and amphidynamic (the 2 segments have different rigidities) (Liu et al., 2018). The nomenclature for SFAs is FnHm, where n and m are the number of carbon atoms in the fluorocarbon and hydrocarbon chains, respectively. The perfluorocarbon segment is aerophilic and extremely hydrophobic and lipophobic, while the hydrocarbon segment is less hydrophobic and is lipophilic (Liu et al., 2018; Broniatowski et al., 2004a). Chain lengths of the fluorinated and hydrocarbon segments of the SFAs alter physical properties such as their volatility (Tsagogiorgas and Otto, 2023; Broniatowski et al., 2004a) and their ability to self-assemble into films at the air-liquid interfaces (Broniatowski et al., 2004a, 2004b; Krafft and Riess, 2009). For example, for the F12 series of SFAs (which contain 12 fluorinated carbons), as the hydrocarbon chain segment of the SFA molecule length increases so does its stability at air-liquid interfaces (Broniatowski et al., 2004a). The perfluorocarbon segment appears to have a greater influence on the ability of the molecules to self-assemble into layers at interfaces than the hydrocarbon segment (Krafft and Riess, 2009).

The covalent connection between the 2 segments results in a molecular dipole moment with respect to the main axis (Morgado et al., 2015). The molecular dipole moment increases with increasing F and H chain lengths of the SFA. The dipole moment is important in the self-assembling properties of SFAs and thus formation of films at air-liquid interfaces and influences the volatility of the SFAs, as it impacts the strength of van der Waals interactions between molecules.

Perfluorohexyloctane (F6H8) inhibits the rate of evaporation ($R_{evap}$) of saline in vitro and is slow to evaporate itself (Vittitow et al., 2023; Agarwal et al., 2018). The shorter chain SFA, perfluorobutylpentane (F4H5) has been used as a vehicle to facilitate delivery of cyclosporine (Novaliq announces FDA acceptance of, 2022; Akpek et al., 2023; Sheppard et al., 2021; Wirta et al., 2019) and has a rapid rate of inherent evaporation (Vittitow et al., 2023; Agarwal et al., 2018). However, there are no studies comparing the effect of different chain length SFAs on inhibition of evaporation. The current in vitro study is focused on comparing the inherent rate of evaporation and anti-evaporative properties of various SFAs with Fn equaling 4 and 6 and Hm ranging from 2 to 10 (Fig. 1; Table 1) to evaluate the effect of relative chain length on the anti-evaporative properties of SFAs.

## 2. Methods and materials

### 2.1. Materials

Phosphate buffered saline (PBS) and 1-(Perfluoro-n-hexyl)decane (F6H10) were obtained from Sigma Chemical Company (St. Louis, MO). 1-(Perfluorobutyl)ethane (F4H2) and 1- (Perfluorohexyl)heptane (F6H7) were obtained from Fluoryx Labs, Carson City, Nevada. Vevye (cyclosporine ophthalmic solution) 0.1 %, which consists of cyclosporine 0.1 % in a vehicle containing perfluorobutylpentane (F4H5) and <1.0 % ethanol, was obtained from Pharmaceutical Buyers, Inc, New Hyde Park, New York. Miebo (perfluorohexyloctane ophthalmic solution; F6H8) was obtained from Bausch + Lomb, Rochester, New York.

**Table 1**
Physical properties of semifluorinated alkanes in the current study.

| | Molecular weight (g/mol) | Boiling point (°C) | Vapor pressure (Torr) | Vapor pressure (mm Hg at 20 °C) | Dipole moment (D) |
|---|---|---|---|---|---|
| F4H2 | 246.1 | 58 | | 238[a] | 2.61[b] |
| F4H5 | 290.2 | 134[c] | 25.1 (at 37 °C)[c] | 6.3[b] | 2.81[b] |
| F6H7 | 418.2 | | | | |
| F6H8 | 432.3 | 223[c] | <1 (at 25 °C)[c] | 0.29[d] | 2.99[b] |
| F6H10 | 460.3 | | | | |

[a] National Center for Biotechnology Information. PubChem Compound Summary for CID 88054, Perfluorobutylethylene. Accessed Apr 7, 2025. https://pubchem.ncbi.nlm.nih.gov/compound/Perfluorobutylethylene.
[b] Morgado et al. (2015)
[c] Tsagogiorgas et al. (Tsagogiorgas and Otto, 2023).
[d] Miebo Safety Data Sheet. Accessed Apr. 7, 2025. https://bauschlomb.cority.com/publicchemproduct/publiclogin.rails?view=1041.

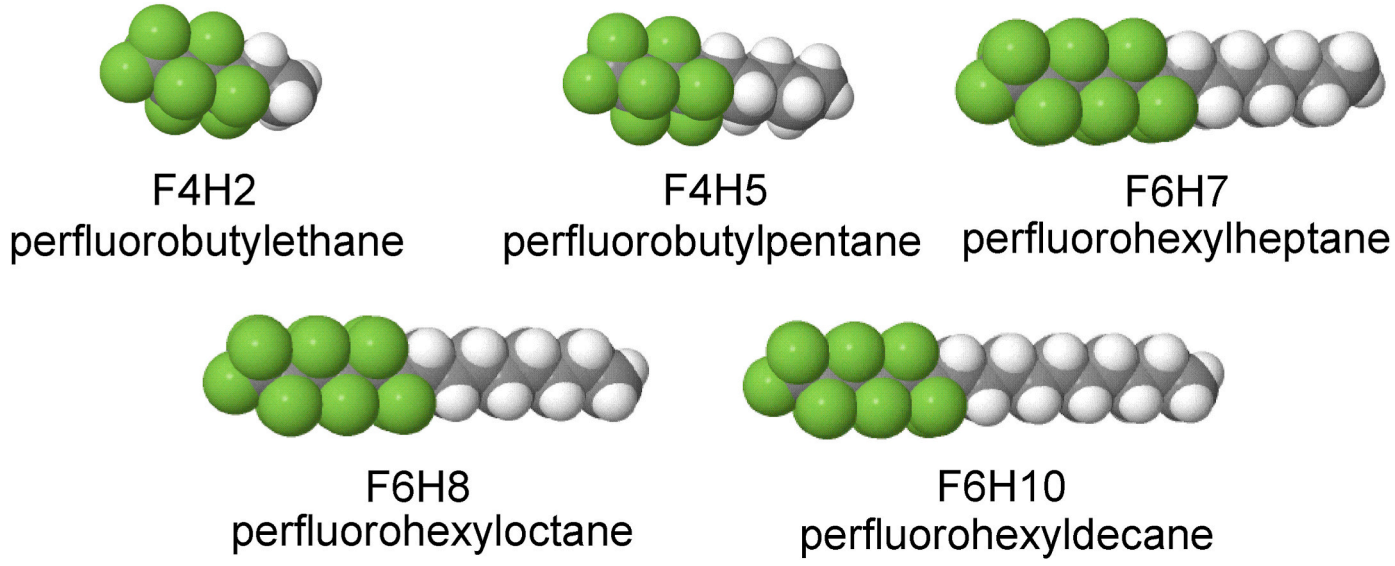


**Fig. 1.** Space-filling models of semifluorinated alkanes examined in the current study. White balls are hydrogen atoms, gray balls are carbon atoms, and green balls are fluorine atoms. The nomenclature for semifluorinated alkanes is FnHm, where n is the number of fluorinated carbons and m is the number of protonated carbons. (For interpretation of the references to color in this figure legend, the reader is referred to the Web version of this article.)

### 2.2. Evaporation rate studies

The $R_{evap}$ was measured gravimetrically as described previously using a Mettler-Toledo XPR225DR analytical balance (Columbus, OH) (Vittitow et al., 2023; Sledge et al., 2016; Borchman et al., 2009, 2013). The balance was calibrated and certified by a Mettler technician. $R_{evap}$ measurements were conducted at 35 °C. To control the temperature of the experiments, samples were placed on an aluminum block, the temperature of which was controlled by water circulating through it from a Haake-B water bath (Haake Manufacturing, DeSoto, MO). PBS was used as a surrogate for human tears, given the $R_{evap}$ of human tears is the same as that of PBS alone (Sledge et al., 2016) and the length of time that would have been required to collect the volume of tears needed prohibited using tears in the current study.

The $R_{evap}$ of PBS and SFAs alone was measured by placing 1 mL each of these molecules into a polyethylene container 0.8 cm deep with an inside diameter of 1.5 cm and $R_{evap}$ measured gravimetrically as reported (Vittitow et al., 2023; Sledge et al., 2016; Borchman et al., 2009, 2013). To evaluate the effect of SFAs on the $R_{evap}$ of PBS, 1 mL PBS alone was placed into a polyethylene container 0.8 cm deep with an inside diameter of 1.5 cm as reported (Vittitow et al., 2023; Sledge et al., 2016; Borchman et al., 2009, 2013). At these dimensions, the surface area of samples within the container, 1.77 $cm^2$, is similar to that of the human ocular surface (Crahay et al., 2022; Millar, 2021). After a 30-min equilibration period at 35 °C, an 11 μL or 100 μL aliquot of SFAs was placed on the surface of a 1 mL sample of PBS. After another 10-min equilibration period at 35 °C, total sample weight was recorded to 5 decimal places every 10 min over 100 min by removing the samples from the aluminium block and weighing on the analytical balance with the door closed over a period of 10 s. Three samples to determine the $R_{evap}$ for PBS alone were included in every experiment as controls and the SFA samples were evaluated on multiple occasions to minimize the effect of differing environmental conditions on different days. Room temperature and relative humidity were recorded for each determination and the study samples were masked to the investigator.

In all experiments, the total $R_{evap}$ for each sample was obtained from the slope of the best-fit line obtained by least squares linear regression analysis expressed in units of g/min. To convert $R_{evap}$ in g/min to $R_{evap}$ in μm/min, the following equation was used:

$$R_{evap}\ (g/min) / density\ (g/mL) \times 1\ cm^3/mL / area\ (cm^2) \times 10^4\ \mu m/cm$$

Where "area" is the surface area of the samples within the container exposed to the air, or 1.766 $cm^2$. A density of 1.000 g/mL was used for PBS (actual density of water is 0.997 $g/cm^3$ at 25 °C). $R_{evap}$ data are presented as the mean ± standard error of the mean (SEM). Evaporation rates of PBS were corrected for rate of evaporation of the SFAs alone. The $R_{evap}$ of PBS was determined by subtracting the $R_{evap}$ of the respective SFAs from the total $R_{evap}$ of the combined sample to generate an adjusted $R_{evap}$ as needed. The percent inhibition of the $R_{evap}$ of PBS by the SFAs was calculated by subtracting the adjusted $R_{evap}$ multiplied by 100 and divided by the $R_{evap}$ of PBS alone from 100. P-values to test for significance were measured using a 2-tailed Student's *t*-test for the $R_{evap}$ of the SFAs alone and a one-way ANOVA with a Bonferroni post-test for multiple comparisons for the $R_{evap}$ of saline with and without SFAs. A p-value $<0.05$ was considered statistically significant.

### 2.3. Fourier transform spectroscopy

A Fourier transform infrared spectrometer (Nicolet iS20; Thermo Fisher Scientific, Inc, Waltham, MA) was used to determine the effect of chain length on the order (fluidity) of the hydrocarbon and fluorocarbon moieties of SFAs. About 50 μL of sample was placed directly in between 2 silver chloride windows and infrared spectra were measured at 25 °C with a resolution of 1 $cm^{-1}$. The symmetric $CH_2$ stretching band near 2850 $cm^{-1}$($\tilde{\nu}_{sym}$) was used to estimate the content of *trans* and *gauche* rotamers in the hydrocarbon chains (Borchman et al., 2007). The more *trans* rotamers, the stronger the hydrophobic interactions and the greater the order or stiffness of the chains. Similarly, the CF band near 1250 $cm^{-1}$ was used to estimate the fluidity of the $CF_2$ fluorocarbon chain. GRAMS/386 software (Galactic Industries, Salem, NH) was used for spectral analysis.

## 3. Results

### 3.1. Evaporation rates

One hundred–weight measurements for each of the trials of 100 min each were made. The relative humidity and room temperature were 32.70 % ± 0.34 % and 25.60 °C ± 0.19 °C, respectively when the $R_{evap}$ was determined. The $R_{evap}$ of the samples alone followed the order F4H2 > F4H5 > F6H7 > F6H8 ≈ F6H10, p = 0.0002, 0.0001, 0.0008, 0.54, respectively (Table 2). The evaporation data indicate 11 μL of sample would evaporate from 0.1 min to 115 min and 100 μL of sample would evaporate from 1 min to 1048 min. All 100 μL of F4H2 evaporated in about 1 min (Table 2).

Measured $R_{evap}$ values were extremely linear, $p < 0.01$, with an average linear correlation coefficient of 0.9980 and 0.9968 for the 11 μL and 100 μL trials, respectively. Layering 100 μL of sample on top of PBS resulted in an inhibition of the $R_{evap}$ of saline (corrected for the $R_{evap}$ of SFA alone) following the order F4H5 ≈ F4H2 < F6H7 < F6H10 < F6H8 (Fig. 2A). Relative to $R_{evap}$ for PBS, 10.53 ± 0.06 μm/min, n = 81, all samples except F4H2 and F4H5 significantly inhibited $R_{evap}$ versus PBS alone ($p < 0.001$). A pilot study of $R_{evap}$ of F4H5 alone indicated that the added 0.1 % cyclosporine and ethanol in the formulation had a negligible effect on $R_{evap}$ (data not shown). In contrast to the F4 series, the F6 series inhibited $R_{evap}$ by 40 %–80 % (Fig. 2A–Table 3). Layering 11 μL of sample (equivalent to 1 drop of F6H8 when dosed on the eye) on top of PBS had less of an effect on $R_{evap}$ compared with layering 100 μL of sample (Fig. 2B; Table 3). An 11 μL drop of F6H8 significantly inhibited $R_{evap}$ by 20.4 % ($p < 0.0001$), while the other SFAs had no significant effect on $R_{evap}$ ($p > 0.09$; Table 3).

The assay measures $R_{evap}$ over a 100-min period. Note that 11 μL of F6H7 did not significantly inhibit $R_{evap}$, while 100 μL of F6H7 resulted in a 40 % inhibition (Table 3; Fig. 2A), likely because alone, 11 μL of F6H7 evaporates in 25 min and 100 μL of F6H7 evaporates in 226 min (Table 2). However, 11 μL of F4H2 did not significantly inhibit $R_{evap}$, while 100 μL of F4H2 also had a negligible effect on the rate of $R_{evap}$ (Table 3), likely because alone it evaporates in seconds (Table 2).

### 3.2. Spectroscopic study

The infrared $CH_2$ symmetric stretching band frequency ($\tilde{\nu}_{sym}$) near 2850 $cm^{-1}$ was used to measure the hydrocarbon segment order (fluidity) of SFAs (Fig. 3). Infrared CF stretching moieties near 1280 $cm^{-1}$ were used to measure the CF segment order (fluidity) of SFAs (Fig. 3). The higher the $\tilde{\nu}_{sym}$, the more disordered (fluid) the chain (see Discussion section).

**Table 2**
Evaporation rates of samples alone at 35 °C.

| | Evaporation rate (g/min, n)[a] | Time to evaporate 100 μL (min) | Time to evaporate 11 μL (min) |
|---|---|---|---|
| F4H2 | 0.102 (0.025), 3 | 1 | 0.1 |
| F4H5 | 0.0060 (0.0006), 6 | 21 | 2.3 |
| F6H7 | 0.00058 (0.00020), 4 | 226 | 25 |
| F6H8 | 0.000150 (0.000017), 9 | 837 | 92 |
| F6H10 | 0.000120 (0.00009), 5 | 1048 | 115 |

[a] Data are expressed as mean (standard error of the mean), number of determinations, n.

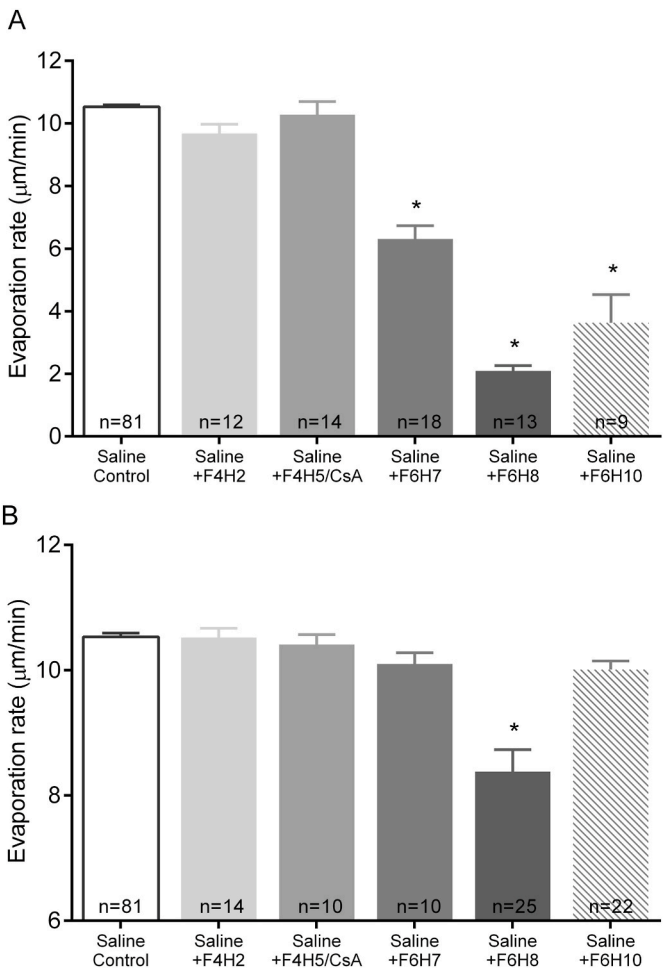


**Fig. 2.** Evaporation rates of phosphate buffered saline with and without 100 µL semifluorinated alkanes (A) or 11 µL semifluorinated alkanes (B) layered on the surface similar to the surface area of the human eye. The F4H5 sample contained 0.1 % cyclosporine. The sample temperature was 35 °C. *p < 0.0001. Error bars are the standard error of the mean; n = number of determinations.

The $CH_2$ and $CF_2$ $\tilde{\nu}_{sym}$ were related to the boiling points (Fig. 4A and C) and dipole moments (Fig. 4B and D) of 3 SFAs using available published data (Table 1). The number of carbons in the hydrocarbon segment were related to $CH_2$ $\tilde{\nu}_{sym}$ (Fig. 4E). The inset bar graph (Fig. 4E) highlights the disproportionate $\tilde{\nu}_{sym}$ of $CH_2$ for F2H4. The number of carbons in the perfluorocarbon segment had a minimal impact on the relative differences in the $CF_2$ $\tilde{\nu}_{sym}$ of the F6 series (Fig. 4F). However, the number of carbons in the perfluorocarbon segment impacted the $CF_2$ $\tilde{\nu}_{sym}$ of the F6 series verses the F4 series (Fig. 4F).

The $\tilde{\nu}_{sym}$ for $CF_2$ and $CH_2$ of the evaluated SFAs increased with decreasing chain length (Fig. 5A) and was related to $R_{evap}$ (Fig. 5B–D) indicating SFA-SFA interactions were higher with longer chain length. The inherent $R_{evap}$ in Fig. 5B–D were expressed logarithmically as the inherent $R_{evap}$ spanned about 3 orders of magnitude. F4H2 had a relatively low inherent $R_{evap}$ compared with the other SFAs resulting in a less linear relationship with $\tilde{\nu}_{sym}$, so it was plotted separately (Fig. 5D). Fig. 5E illustrates the rotational arrangement of bonds in the hydrocarbon chain. The lower the $CH_2$ frequency, the more *trans* rotamers and the stiffer the carbon chains of SFAs, thus the larger the van der Waals interactions.

## 4. Discussion

The major findings of the current study are: i) the chain lengths and order of the respective perfluorocarbon and hydrocarbon segments of the SFAs dramatically alter the efficacy of the molecules in terms of their anti-evaporative effect; ii) hydrocarbon and fluorocarbon chain lengths were related to the SFAs inherent $R_{evap}$, chain order, dipole moment, and boiling point; iii) the evaluated SFAs had dramatically different anti-evaporative effects and when 11 µL of the SFAs was layered on the surface of saline, only F6H8 inhibited $R_{evap}$ of PBS.

### 4.1. The inherent $R_{evap}$ of SFAs and $CH_2$ and $CF_2$ stretching frequencies

The inherent $R_{evap}$ of SFAs is important to the inhibition of $R_{evap}$ of PBS as SFAs that evaporate quickly will have a briefer ocular surface residence time (Agarwal et al., 2018). Previous in vitro gravimetric analysis comparing the evaporation rate of 500 µL F6H8 directly with F4H5 showed that <1.5 % of F6H8 evaporated by 1 h compared with 93 % of F4H5 (Agarwal et al., 2018). In the current study, the inherent $R_{evap}$ was 680 times greater for F4H2 and 40 times greater for F4H5 compared with F6H8, which is in agreement with the previously reported inherent rate of evaporation of F4H5, which was approximately 50 times greater than that of F6H8 (Agarwal et al., 2018).

Central to the level of inherent $R_{evap}$ is the strength of hydrophobic interactions between the SFA molecules. The strength of hydrophobic van der Waals interactions between SFA molecules was inferred from the C–H and C–F stretching frequencies, $\tilde{\nu}_{sym}$ (Borchman et al., 1991, 1996, 1999, 2004, 2007; Kóta et al., 1999; Moore et al., 1993; Popova and Hincha, 2003; Casal and Mantsch, 1984; Mantsch and McElhaney, 1991; Mendelsohn and Moore, 1998). Simply put, van der Waals interactions are a result of the distortion in the distribution of electric charge in the structure of some molecules. Electron density momentarily migrates from one side of a molecule creating a small negative charge on one side of the carbon chain and a small positive charge on the opposite side (Petrucci, 2007) resulting in a dipole moment that is a result of unequal electron distribution. The transient negative and positive charges result in hydrophobic interactions between carbon chains. The molecular dipole moment with respect to the main axis of the SFA is directly related to the $CH_2$ and $CF_2$ $\tilde{\nu}_{sym}$ (Fig. 5B and D).

When lipids or the carbon chains of SFAs are in a completely ordered state, the $CH_2$ moieties in the hydrocarbon segment are in an all-*trans* conformation (Fig. 5E) allowing the chains to pack more tightly

**Table 3**
Effect of SFAs on rate of evaporation of PBS.

| Test condition | Evaporation rate (µm/min)[a] | Inhibition of evaporation (%) | P-value vs PBS | Evaporation rate (µm/min)[a] | Inhibition of evaporation (%) | P-value vs PBS |
|---|---|---|---|---|---|---|
| Amount added | 100 µL | | | 11 µL | | |
| F4H2 | 9.67 (0.30) n = 12 | 8.2 | 0.81 | 10.52 (0.15) n = 14 | 0.1 | 0.99 |
| F4H5 (plus 0.1 % cyclosporine) | 10.28 (0.42) n = 14 | 2.4 | 0.99 | 10.41 (0.16) n = 10 | 1.1 | 0.99 |
| F6H7 | 6.31 (0.42) n = 18 | 40.1 | <0.0001 | 10.10 (0.18) n = 10 | 4.1 | 0.69 |
| F6H8 | 2.09 (0.17) n = 13 | 80.2 | <0.0001 | 8.38 (0.35) n = 25 | 20.4 | <0.0001 |
| F6H10 | 3.63 (0.90) n = 9 | 65.5 | <0.0001 | 10.01 (0.14) n = 22 | 4.9 | 0.07 |
| PBS alone (control) | 10.53 (0.06), 81 | | | | | |

[a] Data are expressed as mean (standard error of the mean), n = number of determinations. PBS = phosphate buffered saline; SFA = semifluorinated alkane.

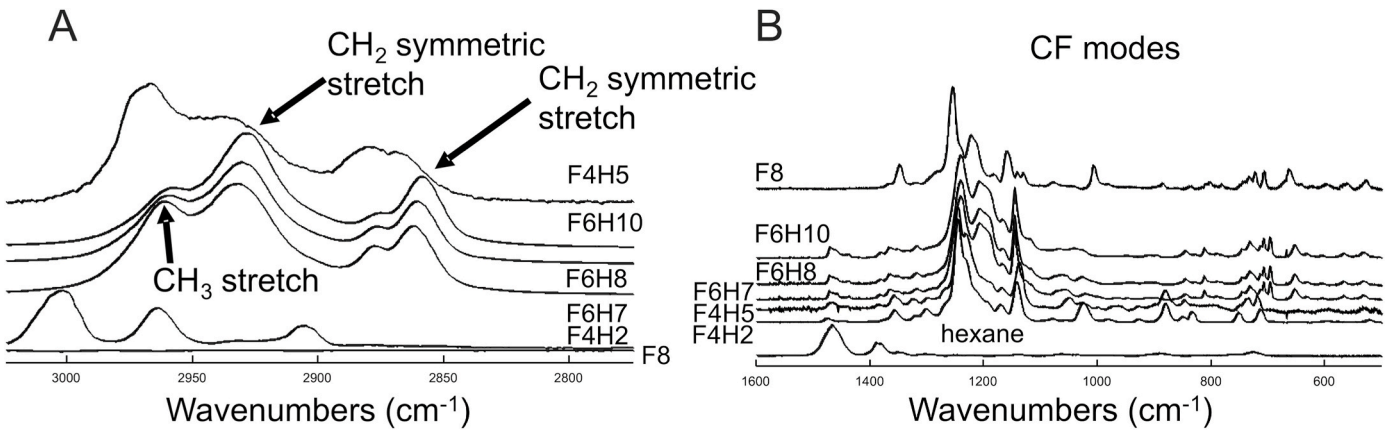


**Fig. 3.** Infrared spectra of semifluorinated alkanes shown in Fig. 1. (A) CH stretching region. (B) CF stretching region.

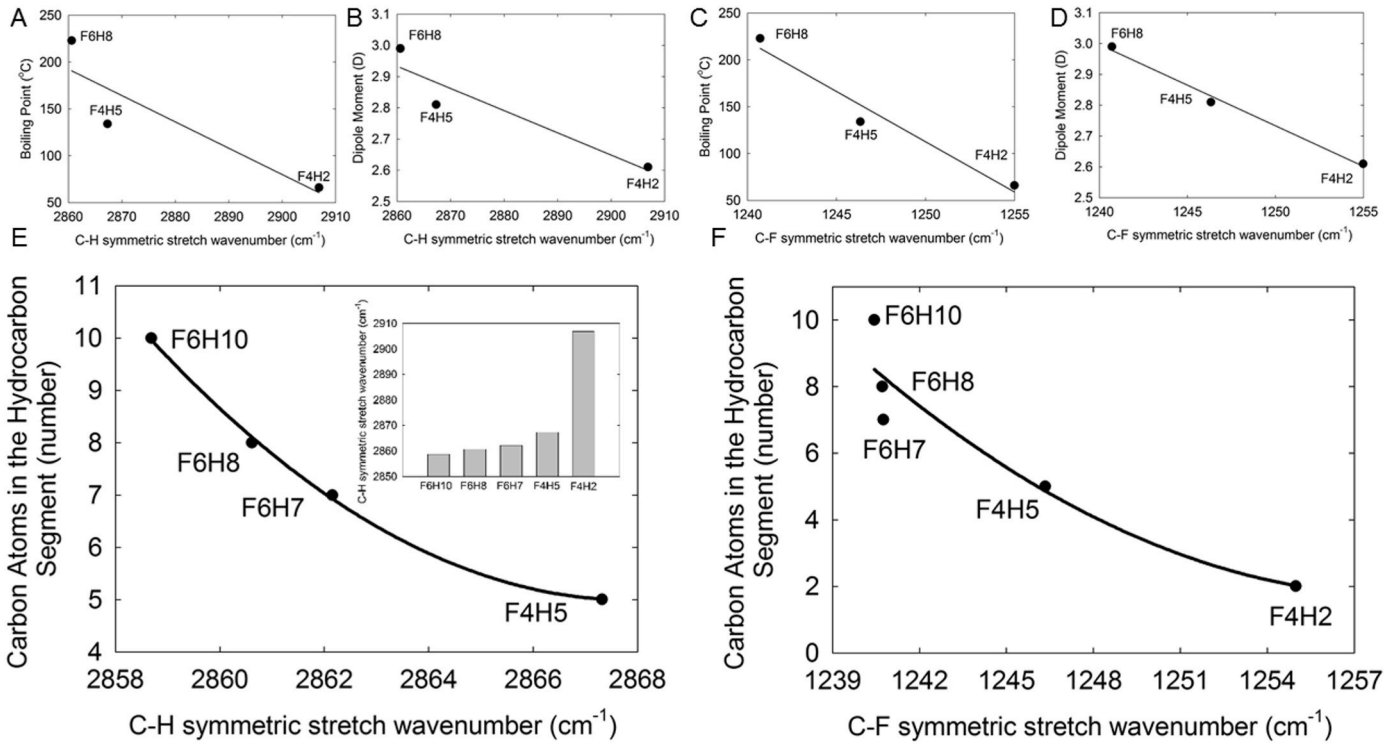


**Fig. 4.** Relationships between C–H symmetric stretching frequency and (A) boiling point, (B) dipole moment, (E) protonated and fluorinated carbons. Relationships between C–F symmetric stretching frequency and (C) boiling point, (D) dipole moment, (F) protonated and fluorinated carbons. The higher the wavenumber, the higher the disorder (fluidity).

maximizing van der Waals interactions. In this instance, the $CH_2$ $\tilde{\nu}_{sym}$ is low as the protons stretch at a lower frequency and hydrophobic interactions between SFA molecules are high. van der Waals forces become smaller and even disappear as the distances between the atoms or molecules increase. More *gauche* rotamers (Fig. 5E) do not allow the chains to pack tightly, reducing van der Waals interactions resulting in higher $CF_2$ and $CH_2$ $\tilde{\nu}_{sym}$ and lower hydrophobic interactions.

The order of the hydrocarbon and fluorocarbon chains measured from $CF_2$ and $CH_2$ $\tilde{\nu}_{sym}$ is related to the log of the inherent $R_{evap}$ of the SFAs alone (Fig. 5B–D). As the hydrocarbon chains of F4H5 and F4H2 are relatively more disordered (as exhibited by a higher $\tilde{\nu}_{sym}$) compared with the F6 series, they evaporate much more quickly than the F6 series. The infrared $CF_2$ and $CH_2$ $\tilde{\nu}_{sym}$ are also related to the boiling point and dipole moment of the SFAs based on published data available for F4H2, F4H5, and F6H8 (Fig. 4; Table 1). The $CH_2$ $\tilde{\nu}_{sym}$ is related to the number of carbons in the hydrocarbon segment (Fig. 4E). As the number of carbons in the hydrocarbon segment increases, van der Waals interactions become larger. The $CF_2$ $\tilde{\nu}_{sym}$ also is related to the F4 and F6 series but not the F6 series alone (Fig. 4F), perhaps because of how the F6 series is structurally arranged. The infrared $CF_2$ and $CH_2$ $\tilde{\nu}_{sym}$ (fluidity) of F4H2 are relatively high (Fig. 4E inset, F), suggesting F4H2–F4H2 interactions are minimal.

In summary, the hydrocarbon and perfluorocarbon segment order of the F6 series is much greater compared with the F4 series, which causes the F4 series to have a lower boiling point and van der Waals interaction and to evaporate more quickly than the F6 series.

### 4.2. *Effect of SFAs on $R_{evap}$ of saline*

The $R_{evap}$ of PBS measured in the current study was 10.53 ± 0.06 μm/min, n = 81. This value was not significantly different, p = 0.65, from the value previously measured at 35 °C, 10.47 ± 0.008 μm/min, n

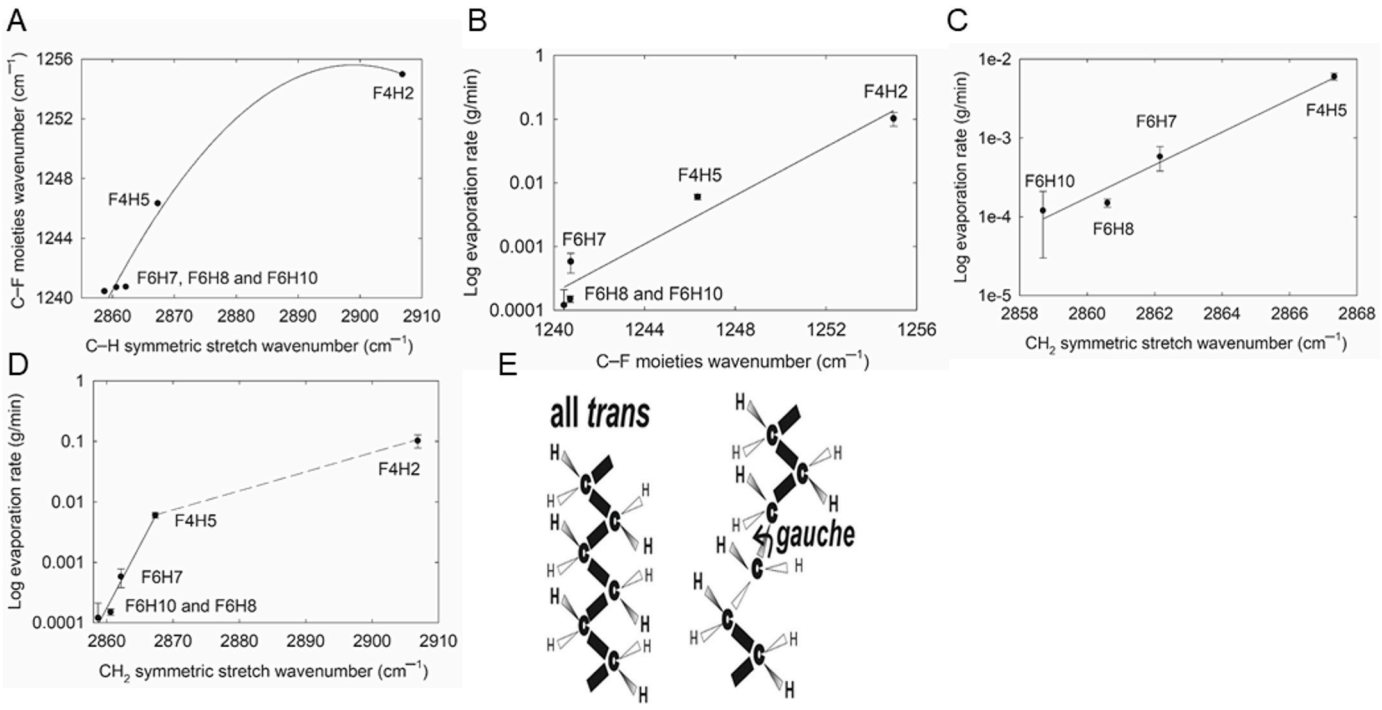


**Fig. 5.** The (A) $CH_2$ and CF stretching frequencies of the semifluorinated alkanes in Fig. 1 increased with increasing hydrocarbon chain length indicating SFA–SFA interactions decreased and were related to the log of the rate of evaporation (B, C, and D). (E) Hydrocarbon chain conformation is dependent on the rotational arrangement of bonds. The lower the $CH_2$ frequency, the more *trans* rotamers and the stiffer the lipid, the larger the van der Waals interactions.

= 16, (Vittitow et al., 2023) or 9.9 ± 0.1 μm/min, n = 8, measured 1 °C lower, 34 °C, p = 0.23 (Sledge et al., 2016).

When 11 μL of the SFAs was layered on the surface of saline, only F6H8 significantly inhibited $R_{evap}$, by 20.4 % ($p < 0.0001$). Similarly, when 100 μL of SFAs was layered on top of saline, only the F6 series significantly inhibited the $R_{evap}$, with F6H8 resulting in the greatest inhibition of evaporation. The magnitude of anti-evaporative effect of F6H8 is consistent with results from a previous study in which 100 μl and 11 μl of F6H8 resulted in 80 % and 28 % inhibition of $R_{evap}$ respectively (Vittitow et al., 2023). Among the F6 series, at 100 μL of surface SFA, F6H8 and F6H10 had a greater inhibitory effect on $R_{evap}$ compared with F6H7.

It is likely that the F4 series had no significant effect on the inhibition of $R_{evap}$ of saline because the F4 series has a very rapid rate of inherent evaporation, such that when layered on an aqueous surface there is only a brief residence time. Eleven microliters of F4H2, F4H5, and F6H7 evaporated in 0.1, 1, and 25 min, respectively, much quicker than the 100 min of the assay $R_{evap}$ measurement. In addition, the SFA-SFA van der Waals interactions are much weaker for the F4 series, which would allow water to pass through between the molecules of the SFA. The dipole moment values for F4H2, F4H5, and F6H8 (Table 1) are consistent with the greater anti-evaporative properties of F6H8 versus the 2 SFAs with shorter chain length, F4H2 and F4H5.

With respect to the F6 series of SFAs, the reason that F6H8 had a greater anti-evaporative effect than F6H7 may be because the hydrocarbon chain of F6H7 is much more disordered (higher $CH_2$ $\tilde{\nu}_{sym}$, Fig. 5E) compared with F6H8 and evaporates much more quickly. Thus, there is a strong correlation between the inherent $R_{evap}$ of the F4 and F6 series of SFAs and effect on inhibition of $R_{evap}$ of PBS. It is less clear why F6H8 resulted in greater inhibition of the $R_{evap}$ of PBS than F6H10. The difference is not due to perfluorocarbon segment order (Fig. 5E) or the $R_{evap}$ of the SFA alone (Table 1), as these parameters are similar. Perhaps the reason F6H8 inhibited the $R_{evap}$ and F6H10 does not, may be because the hydrocarbon segment of F6H10 is more ordered (lower C–H stretching frequency, Fig. 4E) and the SFA forms a less uniform, more aggregated layer.

The in vitro gravimetric assay used in the current study is an established model (Vittitow et al., 2023; Sledge et al., 2016; Borchman et al., 2009, 2013), however there are several limitations of the methodology, including controlling for variations in environmental conditions. Fluctuations in ambient room humidity and airflow in addition to sample temperature, all impact evaporation rate as outlined in a seminal paper evaluating the effect of meibum on water evaporation in vitro (Cerretani et al., 2013). To mitigate these potential environmental confounders, three control PBS samples (without SFA) were run alongside the SFA test samples in every experimental run, the SFAs were compared to PBS on different days and the overall mean values are reported. In addition, the relative ambient conditions were monitored each day the $R_{evap}$ was evaluated and were relatively constant (mean [SD] of 32.70 % [0.34 %] and 25.60 °C [0.19 °C], respectively). The experimental runs were conducted following equilibration of the samples to 35 °C to mimic the ocular surface temperature. The accuracy of the assay was very good as the $R_{evap}$ values were extremely linear, $p < 0.01$, with an average linear correlation coefficient of 0.9980 and 0.9968 for the 11 μL and 100 μL trials, respectively. $R_{evap}$ of PBS from 81 trials was 10.53 ± 0.06 μm/min and is consistent with previous studies using the same methodology (Vittitow et al., 2023; Sledge et al., 2016; Borchman et al., 2009, 2013). The 5 % variation of $R_{evap}$ of PBS from trial to trial in the current study can be attributed to slight day-to-day differences in ambient conditions. As seen from the error bars, the evaporation measurements for all samples were relatively reproducible. Furthermore, the study samples were masked to the investigator to prevent any subjective bias.

As noted by Cerretini et al., sample thickness, conformation, and stability all contribute to evaporative resistance (Cerretani et al., 2013) Since an equal volume of sample was used for each evaluated SFA, the thickness of the SFA layer was equivalent at the start of the assay for all samples. However, consistent with their much higher inherent evaporation rates, the F4 series SFAs were present on the surface for only a brief period and also had a more disordered and fluid molecular structure relative to the F6 series as demonstrated by infrared spectroscopy. Previous studies simulating the formation of SFA films have shown that some SFAs can self-assemble into aggregates of highly organized

hemimicelles on the surface of fluids, with the lipophilic hydrocarbon chain inserted into the aqueous layer and the lipophobic fluorinated chain orientated to the air (Silva et al., 2019, 2024; Piñeiro et al., 2009). Since the chain is much more hydrophobic than the hydrocarbon chain it cannot orientate into the aqueous layer (Silva et al., 2019, 2024; Piñeiro et al., 2009). The assembly process is highly complex and dependent on the chain length of the fluorinated and hydrocarbon segments, dipole moment and physicochemical properties of the individual SFA (Silva et al., 2019, 2024; Piñeiro et al., 2009).

For the F6 series SFAs, given their ability to inhibit evaporation, the expectation is that the molecules in contact with the water will form a stable monolayer over the duration of the assay. It is unknown precisely how the additional molecules on top of this monolayer will orientate themselves into a multilayer structure, but the assumption is that it is less structured than the monolayer in contact with saline below since the molecules lack the stabilizing interaction with the water. In contrast, based on their more disordered structure, high inherent evaporation rates and lack of ability to significantly inhibit $R_{evap}$ of saline, it is not expected that the F4 series can form either a stable monolayer or multilayered structure.

Clinically, 2 of the SFAs evaluated are used in FDA-approved dry eye disease therapeutics. F4H5 is used as the vehicle in cyclosporine ophthalmic solution 0.1 % to improve drug solubilization and thus delivery to the ocular tissues (Agarwal et al., 2018; Novaliq announces FDA acceptance of, 2022). F6H8 is the only component and active ingredient of perflurohexyloctane ophthalmic solution and is an anti-evaporative agent (Sheppard et al., 2023; Tauber et al., 2023; Vittitow et al., 2023). Consistent with the in vitro data demonstrating no effect of F4H5 on evaporation of saline, F4H5 had a brief corneal residence time in an ex vivo model and a rapid inherent rate of evaporation in vitro (Agarwal et al., 2018). In contrast, F6H8 had a 3-fold longer corneal residence time than F4H5 and a much slower rate of evaporation in vitro, with 50 % remaining at 24 h, which aligns with its robust anti-evaporative properties (Agarwal et al., 2018). Moreover, a study in rabbits demonstrated that F6H8 dosed twice daily significantly improved lipid layer grade in a 7-day study while the comparator F4H5 was without effect over this timeframe (Agarwal et al., 2019). Consistent with its lipid stabilizing properties and ability to improve homeostasis of the tear film, F6H8 also significantly increased tear film thickness in a clinical study of patients with Meibomian gland dysfunction (Schmidl et al., 2020).

It should be noted that while the in vitro evaporation assay mimicked the area of the surface of the eye, a limitation is that this static system does not incorporate blinking mechanisms and the complex tear film. Indeed, when evaluated in both a rabbit model and in humans, F6H8 was shown to have a much longer ocular surface residence time compared with the in vitro static conditions of the current study (Millar et al., 2025; Krösser et al., 2025). In the in vivo situation, over time and on blinking it is expected that the monolayer of F6H8 will respread and reform, akin to the lipid layer, with slow drainage via nasolacrimal drainage and evaporation from the ocular surface (Millar et al., 2025; Krösser et al., 2025).

In conclusion, the inherent rate of evaporation of the evaluated SFAs correlated with their anti-evaporative effects, with the F6 series SFAs having longer inherent evaporation rates and greater inhibitory effects. When 11 μL of SFA was layered on the aqueous surface, only F6H8 significantly inhibited $R_{evap}$ of PBS. The hydrocarbon segment and perfluorocarbon segment order was related to the inherent $R_{evap}$, dipole moment, chain length, vapor pressure, viscosity, and boiling point of the SFA alone.

## CRediT authorship contribution statement

**Megan E. Cavet:** Writing – review & editing, Supervision, Project administration, Conceptualization. **Jason L. Vittitow:** Writing – review & editing, Supervision, Project administration, Funding acquisition, Conceptualization. **Douglas Borchman:** Writing – review & editing, Software, Resources, Project administration, Methodology, Investigation, Formal analysis, Data curation.

## Funding

This work was supported by Bausch + Lomb, Bridgewater, NJ, USA and the University of Louisville Grant # OGMN230094.

## Declaration of competing interest

The authors declare the following financial interests/personal relationships which may be considered as potential competing interests: Douglas Borchman reports administrative support and article publishing charges were provided by Bausch & Lomb Americas Inc. Megan E. Cavet reports financial support, administrative support, and article publishing charges were provided by Bausch & Lomb Americas Inc. Jason L. Vittitow reports financial support, administrative support, and article publishing charges were provided by Bausch & Lomb Americas Inc. Douglas Borchman reports a relationship with Bausch & Lomb Americas Inc that includes: consulting or advisory. Megan E. Cavet reports a relationship with Bausch & Lomb Americas Inc that includes: employment and equity or stocks. Jason L. Vittitow reports a relationship with Bausch & Lomb Americas Inc that includes: employment and equity or stocks.

## Acknowledgements

Editorial assistance was provided by Synchrony Medical Communications, LLC, West Chester, PA, and funded by Bausch + Lomb, Bridgewater, NJ, USA.

## Glossary

PBS = phosphate buffered saline; $R_{evap}$ = evaporation rate; SEM = standard error of the mean; SFA = semifluorinated alkane; $\tilde{V}sym = CH_2$ symmetric stretching band frequency.

## Data availability

The datasets generated during and/or analyzed during the current study are available from the corresponding author on reasonable request.

## References

Agarwal, P., Scherer, D., Günther, B., Rupenthal, I.D., 2018. Semifluorinated alkane based systems for enhanced corneal penetration of poorly soluble drugs. Int. J. Pharm. 538, 119–129. https://doi.org/10.1016/j.ijpharm.2018.01.019.

Agarwal, P., Khun, D., Krösser, S., Eickhoff, K., Wells, F.S., Willmott, G.R., et al., 2019. Preclinical studies evaluating the effect of semifluorinated alkanes on ocular surface and tear fluid dynamics. Ocul. Surf. 17 (2), 241–249. https://doi.org/10.1016/j.jtos.2019.02.010.

Akpek, E.K., Wirta, D.L., Downing, J.E., et al., 2023. Efficacy and safety of a water-free topical cyclosporine, 0.1%, solution for the treatment of moderate to severe dry eye disease: the ESSENCE-2 randomized clinical trial. JAMA Ophthalmol. 141 (5), 459–466. https://doi.org/10.1001/jamaophthalmol.2023.0709.

Bacharach, J., Kannarr, S.R., Verachtert, A., et al., 2025. Early effects of perfluorohexyloctane ophthalmic solution on patient-reported outcomes in dry eye disease: a prospective, open-label, multicenter study. Ophthalmol. Ther. 14 (4), 693–704. https://doi.org/10.1007/s40123-025-01097-z.

Borchman, D., 2021. Lipid conformational order and the etiology of cataract and dry eye. J. Lipid Res. 62, 100039. https://doi.org/10.1194/jlr.TR120000874.

Borchman, D., Yappert, M.C., Herrell, P., 1991. Structural characterization of human lens membrane lipid by infrared spectroscopy. Investig. Ophthalmol. Vis. Sci. 32 (8), 2404–2416.

Borchman, D., Cenedella, R.J., Lamba, O.P., 1996. Role of cholesterol in the structural order of lens membrane lipids. Exp. Eye Res. 62 (2), 191–198. https://doi.org/10.1006/exer.1996.0023.

Borchman, D., Tang, D., Yappert, M.C., 1999. Lipid composition, membrane structure relationships in lens and muscle sarcoplasm reticulum membranes. Biospectroscopy

5 (3), 151–167. https://doi.org/10.1002/(SICI)1520-6343(1999)5:3%3C151::AID-BSPY5%3E3.0.CO;2-D.
Borchman, D., Yappert, M.C., Afzal, M., 2004. Lens lipids and maximum lifespan. Exp. Eye Res. 79 (6), 761–768. https://doi.org/10.1016/j.exer.2004.04.004.
Borchman, D., Foulks, G.N., Yappert, M.C., Ho, D.V., 2007. Temperature-induced conformational changes in human tearlipids hydrocarbon chains. Biopolymers 87 (2–3), 124–133. https://doi.org/10.1002/bip.20798.
Borchman, D., Foulks, G.N., Yappert, M.C., Mathews, J., Leake, K., Bell, J., 2009. Factors affecting evaporation rates of tear film components measured in vitro. Eye Contact Lens 35 (1), 32–37. https://doi.org/10.1097/ICL.0b013e318193f4fc.
Borchman, D., Foulks, G.N., Yappert, M.C., et al., 2011. Human meibum lipid conformation and thermodynamic changes with meibomian-gland dysfunction. Investig. Ophthalmol. Vis. Sci. 52 (6), 3805–3817. https://doi.org/10.1167/iovs.10-6514.
Borchman, D., Yappert, M.C., Milliner, S.E., et al., 2013. $^{13}C$ and $^{1}H$ NMR ester region resonance assignments and the composition of human infant and child meibum. Exp. Eye Res. 112, 151–159. https://doi.org/10.1016/j.exer.2013.04.017.
Broniatowski, M., Miñones Jr., J., Dynarowicz-Łatka, P., 2004a. Semifluorinated chains in 2D-(perfluorododecyl)-alkanes at the air/water interface. J. Colloid Interface Sci. 279 (2), 552–558. https://doi.org/10.1016/j.jcis.2004.06.080.
Broniatowski, M., Sandez Macho, I., Miñones Jr., J., Dynarowicz- Łątka, P., 2004b. Langmuir monolayers characteristic of (perfluorodecyl)-alkanes. J. Phys. Chem. B 108 (35), 13403–13411. https://doi.org/10.1021/jp0402481.
Casal, H., Mantsch, H.H., 1984. Polymorphic phase behaviour of phospholipid membranes studies by infrared spectroscopy. Biochim. Biophys. Acta 779 (4), 381–401. https://doi.org/10.1016/0304-4157(84)90017-0.
Cerretani, C.F., Ho, N.H., Radke, C.J., 2013. Water-evaporation reduction by duplex films: application to the human tear film. Adv. Colloid Interface Sci. 197–198, 33–57. https://doi.org/10.1016/j.cis.2013.03.007.
Crahay, F.X., Debellemanière, G., Tobalem, S., Ghazal, W., Moran, S., Gatinel, D., 2022. Quantitative interocular comparison of total corneal surface area and corneal diameter in patients with highly asymmetric keratoconus. Sci. Rep. 12 (1), 4276. https://doi.org/10.1038/s41598-022-08021-6.
Eberwein, P., Krösser, S., Steven, P., 2020. Semifluorinated alkane eye drops in chronic ocular graft-versus-host disease: a prospective, multicenter, noninterventional study. Ophthalmic Res. 63 (1), 50–58. https://doi.org/10.1159/000499158.
Georgiev, G.A., Eftimov, P., Yokoi, N., 2017. Structure-function relationship of tear film lipid layer: a contemporary perspective. Exp. Eye Res. 163, 17–28, 10.1016/j.exer.2017.03.013.
Groß, D., Kaercher, T., 2021. Comparison of the clinical efficacy of three different eye drops for the treatment of dry eye. EC Ophthalmol. 12 (6), 32–44.
Habbe, K.J., Frings, A., Saad, A., Geerling, G., 2023. The influence of a mineral oil cationic nanoemulsion or perfluorohexyloctane on the tear film lipid layer and higher order aberrations. PLoS One 18 (1), e0279977. https://doi.org/10.1371/journal.pone.0279977.
Kóta, Z., Debreczeny, M., Szalontai, B., 1999. Separable contributions of ordered and disordered lipid fatty acyl chain segments to nuCH2 bands in model and biological membranes: a Fourier transform infrared spectroscopic study. Biospectroscopy 5 (3), 169–178. https://doi.org/10.1002/(sici)1520-6343(1999)5:3%3C169::aid-bspy6%3E3.0.co;2-#.
Krafft, M.P., Riess, J.G., 2009. Chemistry, physical chemistry, and uses of molecular fluorocarbon–hydrocarbon diblocks, triblocks, and related compounds—unique "apolar" components for self-assembled colloid and interface engineering. Chem. Rev. 109 (5), 1714–1792. https://doi.org/10.1021/cr800260k.
Krösser, S., Grillenberger, R., Eickhoff, K., Korward, J., Cavet, M.E., Mah, F.S., 2025. Ocular pharmacokinetics and biodistribution of perfluorohexyloctane after topical administration to rabbits. J. Ocul. Pharmacol. Therapeut. 41 (7), 370–377. https://doi.org/10.1089/jop.2025.0056.
Lemp, M.A., Crews, L.A., Bron, A.J., Foulks, G.N., Sullivan, B.D., 2012. Distribution of aqueous-deficient and evaporative dry eye in a clinic-based patient cohort: a retrospective study. Cornea 31 (5), 472–478. https://doi.org/10.1097/ICO.0b013e318225415a.
Liu, X., Riess, J.G., Krafft, M.P., 2018. Self-organization of semifluorinated alkanes and related compounds at interfaces: thin films, surface domains and two-dimensional spherulites. Bull. Chem. Soc. Jpn. 91 (5), 846–857, 10.1246bcsj.20170431.
Mantsch, H.H., McElhaney, R.N., 1991. Phospholipid phase transitions in model and biological membranes as studied by infrared spectroscopy. Chem. Phys. Lipids 57 (2−3), 213–226. https://doi.org/10.1016/0009-3084(91)90077-o.
Mendelsohn, R., Moore, D.J., 1998. Vibrational spectroscopic studies of lipid domains in biomembranes and model systems. Chem. Phys. Lipids 96 (1−2), 141–157. https://doi.org/10.1016/S0009-3084(98)00085-1.
Millar, T., 2021. Surface area of the exposed eye. Investig. Ophthalmol. Vis. Sci. 62 (4), 18. https://doi.org/10.1167/iovs.62.4.18.
Millar, T.J., Vittitow, J., Cavet, M., Ahmed, S., Borchman, D., 2025. In vitro and in vivo visualization of perfluorohexyloctane, an eye drop for dry eye disease, using infrared emissivity. Cornea 44 (3), 350–359. https://doi.org/10.1097/ICO.0000000000003718.
Moore, D.J., Wyrwa, M., Reboulleau, C.P., Mendelsohn, R., 1993. Quantitative IR studies of acyl chain conformational order in fatty acid homogenous membranes of live cells of *Acholeplasma laidlawii* B. Biochemistry 32 (24), 6281–6287. https://doi.org/10.1021/bi00075a023.
Morgado, P., Das, G., McCabe, C., Filipe, E.J.M., 2015. Vapor pressure of perfluoroalkylalkanes: the role of the dipole. J. Phys. Chem. B 119 (4), 1623–1632. https://doi.org/10.1021/jp5109448.
Nagar, S., Ajouz, L., Nichols, K.K., et al., 2023. Relationship between human meibum lipid composition and the severity of meibomian gland dysfunction: a spectroscopic analysis. Investig. Ophthalmol. Vis. Sci. 64 (10), 22. https://doi.org/10.1167/iovs.64.10.22.
Nguyen, A., Naidoo, K.K., Ajouz, L., et al., 2024. Changes in human meibum lipid composition related to the presence and severity of meibomian gland dysfunction. J. Ocul. Pharmacol. Therapeut. 40 (9), 562–570. https://doi.org/10.1089/jop.2024.0063.
Novaliq announces FDA acceptance of the new drug application for CyclaSol for the treatment of dry eye disease. www.novaliq.com/press-releases/2022/10/24/novaliq-announces-fda-acceptance-of-the-new-drug-application-for-cyclasol-for-the-treatment-of-dry-eye-disease/, 2022–. (Accessed 4 January 2023).
Petrucci, R.H., 2007. General Chemistry: Principles and Modern Applications. Chemistry. Prentice Hall.
Piñeiro, A., Prieto, G., Ruso, J.M., Verdes, P.V., Sarmiento, F., 2009. Surface films of short fluorocarbon-hydrocarbon diblocks studied by molecular dynamics simulations: spontaneous formation of elongated hemimicelles. J. Colloid Interface Sci. 329 (2), 351–356. https://doi.org/10.1016/j.jcis.2008.10.018.
Popova, A.V., Hincha, D.K., 2003. Intermolecular interactions in dry and rehydrated pure and mixed bilayers of phosphatidylcholine and digalactosyldiacylglycerol: a Fourier transform infrared spectroscopy study. Biophys. J. 85 (3), 1682–1690. https://doi.org/10.1016/S0006-3495(03)74598-6.
Schmidl, D., Bata, A.M., Szegedi, S., et al., 2020. Influence of perfluorohexyloctane eye drops on tear film thickness in patients with mild to moderate dry eye disease: a randomized controlled clinical trial. J. Ocul. Pharmacol. Therapeut. 36 (3), 154–161. https://doi.org/10.1089/jop.2019.0092.
Sheppard, J.D., Wirta, D.L., McLaurin, E., et al., 2021. A water-free 0.1% cyclosporine a solution for treatment of dry eye disease: results of the randomized phase 2B/3 ESSENCE study. Cornea 40 (10), 1290–1297. https://doi.org/10.1097/ICO.0000000000002633.
Sheppard, J.D., Kurata, F., Epitropoulos, A.T., Krösser, S., Vittitow, J.L., MOJAVE Study Group, 2023. NOV03 for signs and symptoms of dry eye disease associated with meibomian gland dysfunction: the randomized phase 3 MOJAVE study. Am. J. Ophthalmol. 252, 265–274. https://doi.org/10.1016/j.ajo.2023.03.008.
Silva, G.M.C., Morgado, P., Lourenço, P., Goldmann, M., Filipe, E.J.M., 2019. Spontaneous self-assembly and structure of perfluoroalkylalkane surfactant hemimicelles by molecular dynamics simulations. Proc. Natl. Acad. Sci. U. S. A. 116 (30), 14868–14873. https://doi.org/10.1073/pnas.1906782116.
Silva, P., Silva, G.M.C., Morgado, P., Fauré, M.C., Goldmann, M., Filipe, E.J.M., 2024. Origin of the central pit in hemimicelles of semifluorinated alkanes: how molecular dipoles and substrate deformation can determine supra-molecular morphology. J. Colloid Interface Sci. 655, 576–583. https://doi.org/10.1016/j.jcis.2023.11.007.
Sledge, S.M., Khimji, H., Borchman, D., et al., 2016. Evaporation and hydrocarbon chain conformation of surface lipid films. Ocul. Surf. 14 (4), 447–459. https://doi.org/10.1016/j.jtos.2016.06.002.
Steven, P., Scherer, D., Krösser, S., Beckert, M., Cursiefen, C., Kaercher, T., 2015. Semifluorinated alkane eye drops for treatment of dry eye disease–A prospective, multicenter noninterventional study. J. Ocul. Pharmacol. Therapeut. 31 (8), 498–503. https://doi.org/10.1089/jop.2015.0048.
Steven, P., Augustin, A.J., Geerling, G., et al., 2017. Semifluorinated alkane eye drops for treatment of dry eye disease due to meibomian gland disease. J. Ocul. Pharmacol. Therapeut. 33 (9), 678–685. https://doi.org/10.1089/jop.2017.0042.
Tauber, J., Wirta, D.L., Sall, K., Majmudar, P.A., Willen, D., Krösser, S., SEECASE study group, 2021. A randomized clinical study (SEECASE) to assess efficacy, safety, and tolerability of NOV03 for treatment of dry eye disease. Cornea 40 (9), 1132–1140. https://doi.org/10.1097/ICO.0000000000002622.
Tauber, J., Berdy, G.J., Wirta, D.L., et al., 2023. NOV03 for dry eye disease associated with meibomian gland dysfunction: results of the randomized phase 3 GOBI study. Ophthalmology 130 (5), 516–524. https://doi.org/10.1016/j.ophtha.2022.12.021.
Tsagogiorgas, C., Otto, M., 2023. Semifluorinated alkanes as new drug carriers—an overview of potential medical and clinical applications. Pharmaceutics 15 (4), 1211. https://doi.org/10.3390/pharmaceutics15041211.
Vittitow, J., Kissling, R., DeCory, H., Borchman, D., 2023. In vitro inhibition of evaporation with perfluorohexyloctane, an eye drop for dry eye disease. Curr. Ther. Res. Clin. Exp. 98, 100704. https://doi.org/10.1016/j.curtheres.2023.100704.
Wirta, D.L., Torkildsen, G.L., Moreira, H.R., et al., 2019. A clinical phase II study to assess efficacy, safety, and tolerability of waterfree cyclosporine formulation for treatment of dry eye disease. Ophthalmology 126 (6), 792–800. https://doi.org/10.1016/j.ophtha.2019.01.024.